Advanced LiDAR

http://publish.mersin.edu.tr/index.php/lidar/index

e-ISSN 2791-8572

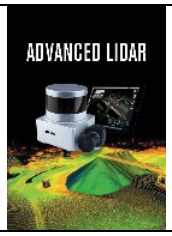

Analysis of Gümüşhane-Trabzon Highway Slope Static and Dynamic Behavior Using Point Cloud Data

Şener Ali Yazıcıoğlu[1], Kaşif Furkan Öztürk[2], Mehmet Akif Günen*[3]

[1]Gümüşhane University, Department of Mining Engineering, 29000, Gümüşhane, Türkiye; (s.aliyazicioglu@gumushane.edu.tr)
[2]Gümüşhane University, Department of Civil Engineering, 29000, Gümüşhane, Türkiye; (kasiffurkan.ozturk@gumushane.edu.tr)
[3]Gümüşhane University, Department of Geomatics Engineering, 29000, Gümüşhane, Türkiye; (akif@gumushane.edu.tr)

Keywords

Photogrammetry,
Slope stability,
Point cloud,
Dynamic analysis.

Research Article

Received : 15.09.2023
Revised : 20.09.2023
Accepted : 26.09.2023
Published : 30.09.2023

* **Corresponding Author**
akif@erciyes.edu.tr

Abstract

It is common knowledge that snowmelt, excessive precipitation, naturally occurring or man-made faulty applications, and static loading conditions can weaken slope stability, which can result in numerous fatalities and property damage. Then again, it is referred to that a few disastrous earthquakes, for example, 1999 Izmit (Mw=7.1), 2023 Pazarcık (Mw=7.7) and Elbistan (Mw=7.6) that happened because of the way that our country is situated in the earthquake belt trigger the slope stability. Within this scope, the mass moves that might happen on the slopes because of the earthquake might cause loss of life and property as well as prevention of road transport. In light of the earthquake, it is critical to guarantee that intercity highways will continue to be serviceable. In this paper, a 3D point cloud was made utilizing photogrammetrically high-resolution aerial photographs and a primer examination of a selected slope system was performed in the Zigana region of the Gümüşhane-Trabzon highway (the previous Zigana Tunnel 5 km). The noise of the point cloud made by utilizing morphological and statistical sorting filters is excluded. Within the relevant point cloud, a section was created from the 3D surface of a region. By using this section, slope stability analysis were implemented for static and dynamic loading situations of the slope by taking into account some foundation rock parameters that are thought to represent the region. In this study, the effect of earthquake induced dynamic analyses on stability were investigated comparatively. As a result of the selected parameters, it is observed that the road slopes that appear to be stable can become unstable especially with the earthquake effect.

1. Introduction

The stability of slopes may deteriorate due to various reasons in nature. Some of these may occur due to natural causes such as strong earthquakes, weathering of rocks or soils, increase in pore water pressure caused by excessive rainfall or water saturation of soils that are not saturated with water, while some of them may occur due to unconscious engineering activities.

It may cause failure of slope stability systems that are already significantly stable or moderately stable under seismic loading (Kramer, 1996). Earthquakes may create greater damage to building systems than their current effects due to loss of slope stabilities (Youd, 1987; Wilson and Keefer, 1985). It has been observed that the loss of life in the major earthquakes that took place in Japan between 1964 and 1980 was largely due to landslides triggered by earthquakes (Kobayashi, 1981). The Haiyuan earthquake in China triggered hundreds of landslides and caused more than 100,000 deaths. During the 1999 Düzce earthquake, a landslide that took place in the Bakacak region, approximately 15 km west of Bolu province, caused an almost 100 m long section slide of the highway and spread over the valley (Bakir and Akiş, 2001). For this reason, transportation was disrupted for a few days until an alternative route was opened (Erdik, 2001). Technical reports prepared on the Pazarcık (Mw=7.7) and Elbistan (Mw=7.6) earthquakes that occurred in 2023 revealed slope stability problems ranging from a few meters to hundreds of meters in length (Çetin et al., 2023).

Cite this;

Yazıcıoğlu, A. Ş., Öztürk, F. K. & Günen, M. A. (2023). Analysis of Gümüşhane-Trabzon Highway Slope Static and Dynamic Behavior Using Point Cloud Data. Advanced LiDAR, 3(2), 70-75.

Slope stability systems can generally be considered in two ways. First of these is to analyze the slope stability in case of static loading. In such a case, the balance of system is generally associated with external loading/unloading operations in ground system's own weight. In the second of these, in addition to static loading, the slope stability system is investigated by assuming that slopes are exposed to dynamic loading. In this case, it is possible to define the frequently preferred methods under two headings: a) limit equilibrium method and b) numerical methods based on finite elements or finite differences.

For both methods, factor of safety for slopes can be determined. In both approaches, the situation regarding slope safety can be determined by calculating the factor of safety. In many studies conducted in this context, it is often observed that while stability analyzes of ground systems are carried out, whether the slope is generally safe or not is examined by calculating the factor of safety for slopes (Dawson et al., 1999; Matsui and San, 1992).

The analyzes carried out within the scope of the study consist of two parts: static and pseudo-static analyses. In parametric analyses, two different rock properties were taken into account for the slope system. These expressed rock parameters were chosen based on the assumption that the slope system consists of limestone or andesitic basaltic tuff, which is known to be common in the region. Comparisons were implemented using total displacements and system's factor of safety for three node points determined from slope section produced using the data obtained from the point cloud.

2. Method

In this study, parametric analyzes were carried out with the slope section obtained using photogrammetrically produced point cloud data in the Old Zigana Tunnel region (Gümüşhane side). To produce photogrammetric data of the study area, 11 aerial images taken by the General Directorate of Mapping with an UltraCam Eagle M3 camera in 2018 were used. Each image is 13080x20010 pixels in size and the camera calibration parameters presented with the images were used in the point cloud production stage. In order to carry out the geo-referencing process of the data, geographical data collection was carried out at each point, a minimum of 10 epochs, with the GeoMax Zenith15 GNSS receiver on the sharp edges of the concrete structures that have not been deteriorated or changed since 2018 in the study area. The created point cloud has a ground sampling interval of 12 cm. Error values of 4 control points not used in the photogrammetric balancing process are presented in Table 1. The solid and digital terrain model representing the study area is given in Figure 1.

Table 1. Total error values of control points

	X	Y	Z
Total Error (m)	0.04	0.07	0.2

After the points representing the digital land surface covering the study area were obtained, the noisy data in the point cloud was filtered and cleaned and then transferred to the CAD environment to perform the cross-section creation process. The raw point cloud must be filtered to perform more meaningful data analysis and processing. Additionally, the point cloud must be filtered to preserve existing details such as edge features and achieve the smooth surfaces needed to produce realistic digital models of physical objects (Günen and Beşdok, 2021). For noise removal, the statistical outlier method developed by Rusu and his colleagues (Rusu et al., 2007), which assumes that the distance between a certain point and its neighbors is normally distributed, was first used. For each pi point (i=1…n) in the data set, the average ri distance is calculated by taking into account the K-nearest neighbors (K-nn). This value is evaluated using the sigma rule on the entire dataset, meaning if the result is not within N standard deviations from the mean, then the point is treated as an variance. Assuming that the average distance to K-nn is normally distributed, the standard deviation multiplier can be selected according to the cumulative distribution function from the normal distribution.

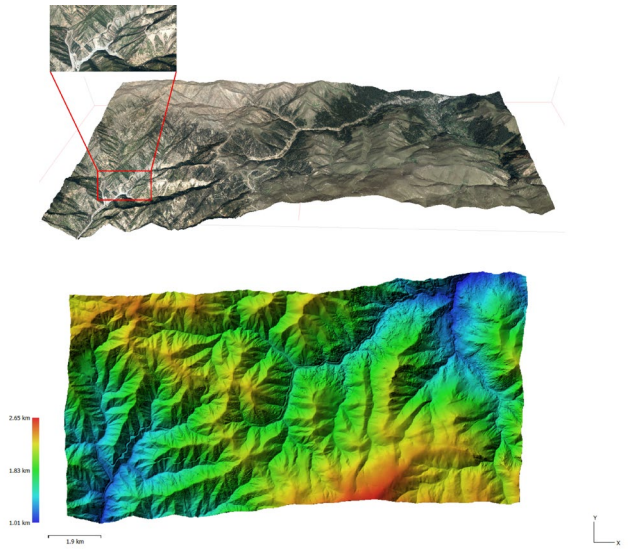

Figure 1. 3D models of the working area

Then, a morphological filter was applied to the point cloud. Morphological filtering methods often rely on extensions of digital image operators adapted to process point elevation rather than grayscale intensity. Morphological filters analyze the shapes and structures of objects in the point cloud. These filters are often used in opening and closing steps to remove small details and noise present in the point cloud. Opening is used to remove small objects or details. Closing is used to preserve the shapes and boundaries of large objects. These steps help to obtain a clearer and cleaner point cloud by determining the shapes of objects in the point cloud more accurately. In the progressive morphology filtering method used in this study, the filtering process depends on the window size and height difference threshold. As a result of an iterative process, points of outer place objects of different sizes are removed from the data set while preserving the ground data (Tan et al., 2018, Wang et al., 2014). Figure 2 shows the trimmed point cloud of the study area and the solid model

representation of the point cloud that was spatially sampled again after filtering.

The rock data used in parametric analyzes were considered as limestone and andesitic basaltic tuff, which are known to be common in the region (Korkmaz, 1988). The physical and mechanical properties used for rock parameters are given in the Table 2. Additionally, poisson ratio were considered as 0.23 and 0.26 for limestone and andesitic basaltic tuff, respectively (Briaud, 2013; Alkan and Dağ, 2018).

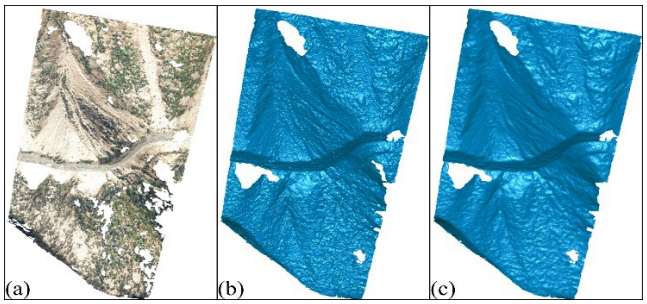

Figure 2. a) Colored b) 2m resolution c) filtered solid model of the working area

Table 2. Rock parameters used in analysis (Korkmaz, 1988)

Rock Type	E_{dyn}, MPa	c, MPa	ϕ (°)	γ, kN/m^3
Limestone	61978	25.497	50	27.26
Andesitic basaltic tuff	28341	17.161	46	25.95

E_{dyn}: Dynamic modulus of elasticity, c: Cohesion, ϕ: Angle of internal friction, γ: Unit volüme weight

2.1. Finite Element Analysis

The finite element method (Bentley, 2020) was used in the stability analysis of the slope system. Two stages were followed in the analyses performed. In the first stage (initial stage), the behavior of the slope system under its own weight was performed by gravity weight. By preserving the effective stresses produced using this approach, in the second stage, the unusual deformations occurring in the slope system are reset and safety analysis is performed to calculate the factor of safety coefficient. Starting from the initial stage, in addition to pseudo-static analyses, analyses were carried out for the factor of safety gradually. In pseudo-static analyses, pseudo-acceleration coefficients are multiplied by g=9.81 m/s^2 and applied to the center of gravity of the area with sliding potential. With this approach, the slope system that will be exposed to earthquake is loaded by "g". It can be considered that horizontal acceleration coefficient (kh) for "large" earthquakes is 0.1, for "severe, destructive" earthquakes is 0.2 and for disaster level is 0.5. In this context within the scope of the study, pseudo-static analyzes were carried out, regarding as 0.1g increments from 0.1g to 0.5g.

Nonlinear behavior of the rocks was considered with the Mohr-Cloumb elasto-plastic material model in the analyses. In the expressed material model, in addition to mechanical properties such as modulus of elasticity and Poisson's ratio, which are frequently used for the linear behavior of the material; cohesion, internal friction angle and dilation angle must be included. Within the scope of the study, dilation angle was accepted as zero. The side boundaries and base of the model were enlarged to eliminate convergence problems, and base was assumed to be the bedrock. While horizontal movement is not allowed at the nodes on the sides, the movement of the nodes on the base is kept in all directions. The network distribution used in the analysis and the nodes where the responses are obtained in the model are presented in Figure 3 and Figure 4, respectively.

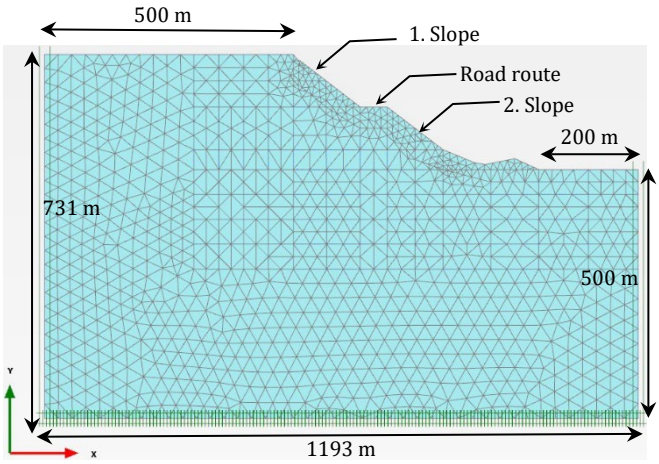

Figure 3. Network distribution for slope model

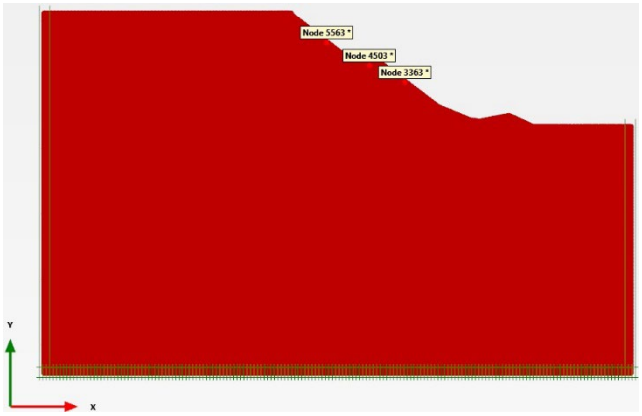

Figure 4. Selected nodes

3. Results and Discussion

3.1. Displacements Obtained from Pseudo-Static Analyzes

The relationship between the largest displacements and loadings obtained from selected nodes in the slope system using limestone and andesitic basaltic tuff system is presented in Figure 5 and Figure 6, respectively. It is clearly understood that the changes generally show an increasing trend in both ways depending on the increase in loadings.

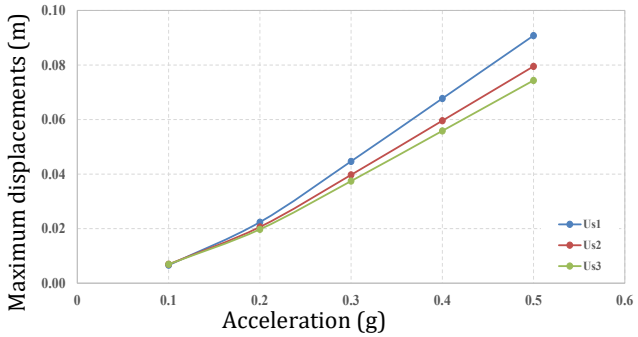

Figure 5. The relationship between the largest displacements and loadings obtained from the selected nodes for limestone

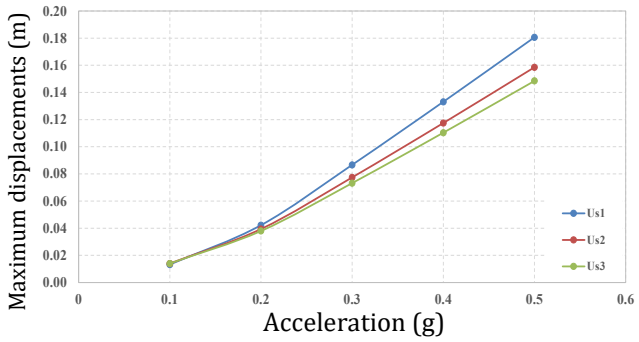

Figure 6. The relationship between the largest displacements and loadings obtained from selected nodes for andesitic basaltic tuff

Table 3. Displacements derived from limestone

Acceleration	Us1(m)	Us2(m)	Us3 (m)
0.1g	0.007	0.007	0.007
0.2g	0.022	0.021	0.020
0.3g	0.045	0.040	0.037
0.4g	0.068	0.060	0.056
0.5g	0.091	0.080	0.074

g=9.81 m/s^2,
Us1:the largest displacement obtained from the node no. 5563,
Us2:the greatest displacement obtained from the node no. 4503,
Us3=the greatest displacement obtained from the node no. 3363

Table 4. Displacements obtained from andesitic basaltic tuff

Acceleration	Us1(m)	Us2(m)	Us3 (m)
0.1g	0.013	0.014	0.014
0.2g	0.042	0.039	0.038
0.3g	0.087	0.077	0.073
0.4g	0.133	0.117	0.110
0.5g	0.181	0.159	0.149

It is observed that under the applied loading, the displacements in the slope system for limestone and andesitic basaltic tuff increase significantly, showing a general trend (Figure 5 and Figure 6). For example, while the Us1 displacement obtained from the 1st slope system using limestone was around 0.007 m under 0.1g loading, it is seen that the same response was obtained as 0.045 and 0.091 m, with an increase of 543% and 1200% under 0.3g and 0.5g loading, respectively (Table 3). Another example of this situation can be given using the Us2 or Us3 displacements in Table 3. For example, while the Us3 displacement obtained from the 2nd slope system was 0.007 m under 0.1g loading, the same response was obtained as 0.037 m and 0.074 m with an increase of 429% and 957% under 0.3g and 0.5g loading, respectively.

The largest displacements obtained from pseudo-static analyzes carried out in the slope system, considering andesitic basaltic tuff, are presented in Table 4. As can be clearly understood here, the increase in loading generally significantly increases the largest displacements obtained from selected nodes. For example, while the Us1 displacement obtained from the 1st slope system is 0.013 m under 0.1g loading, the same displacement becomes 0.087 m and 0.181 m with an increase of 569% and 1292% under 0.3g and 0.5g loading, respectively. It is possible to obtain a similar increasing trend within the selected node on the route. For example, while the Us2 displacement is 0.014 m under 0.1g loading, the same displacement value is obtained as 0.077 m and 0.159 m under 0.3g and 0.5g loadings, increasing by 450% and 1036%, respectively.

Another point that should be emphasized here is that the displacements obtained from the selected nodes, considering limestone and andesitic basaltic tuff, vary significantly compared to each other. For example, while the Us1 displacement was obtained as 0.007 m under 0.1g loading for limestone, this displacement for the same loading was achieved around 0.013 m for andesitic basaltic tuff, with an increase of 86% due to the decrease in the mechanical properties of the rock system and the unit volume weight. This change shows a similar trend, increasing by 93% and 99% under 0.3g and 0.5g loadings, respectively. (Table 3 and Table 4).

3.2. Factor of Safety Coefficient Obtained Under Loadings

The changes in the security numbers obtained from the analyzes are shown in Figure 7 and Figure 8. When Figure 7 and Figure 8 are examined, it is understood that the safety numbers obtained from limestone and andesitic basaltic tuff show a continuous downward trend from the static loading condition in the slope system to the 0.5g loading condition. In order to obtain a constant value of safety numbers in the slope system, it is seen that 100 steps for limestone and 1000 steps for andesitic basaltic tuff are sufficient under loading conditions.

The factor of safety obtained from the analyzes carried out using limestone and andesitic basaltic tuff for the slope system are shown in Table 5. When Table 5 is analyzed, it is clearly seen that the decreasing trend of safety numbers from static loading to pseudo-static loading. For example, while the factor of safety for slope system created from limestone is around 29.33 in static condition, it is seen that the same factor of safety is obtained at 21.62, 13.45 and 9.51 with a decrease of 26%, 54% and 67.5% under 0.1g, 0.3g and 0.5g loadings, respectively. It is possible to see a similar decreasing trend in the slope system created from the andesitic basaltic tuff system. For example, while the static factor of safety for andesitic basaltic tuff is 21.60, this value is

obtained around 16.14, 9.99 and 7.10 with a decrease of 25%, 54% and 67% under 0.1g, 0.3g and 0.5g loadings, respectively.

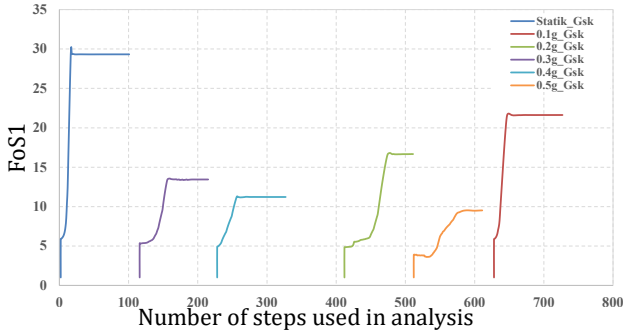

Figure 7. Relationships between step numbers and factor of safety used in the analyzes carried out considering limestone

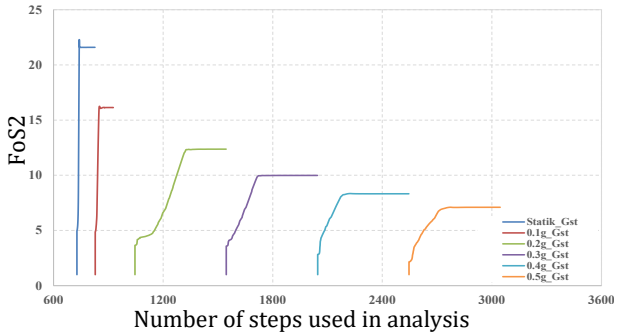

Figure 8. Relationships between step numbers and factor of safety used in the analyzes carried out considering andezitic basaltic tuff

Table 5. Factor of safety obtained from limestone and andesite-basaltic tuff

Acceleration	Gsk	Gst
Statik	29.33	21.60
0.1g	21.62	16.14
0.2g	16.66	12.37
0.3g	13.45	9.99
0.4g	11.22	8.32
0.5g	9.51	7.10

FoS1: Factor of safety for the section obtained from the analyzes performed under the loading considered for limestone
FoS2: Factor of safety for the section obtained from the analysis carried out under the loading considered for andesitic basaltic tuff rock

When a comparison is made between the FoS values obtained for limestone and andesitic basaltic tuff, it is clearly seen that the FoS values obtained from limestone are greater than the FoS values obtained for andesitic basaltic tuff for all loading conditions (Table 5). For example, while the FoS values obtained from andesitic basaltic tuff for the static situation is 21.60, it is seen that the same FoS value is 29.33. In this example, it can be seen that the FoS value obtained from limestone has increased by around 36% compared to the FoS value obtained from andesitic basaltic tuff. Similar changes can be easily observed in pseudo-static loading. For example, if we look at the FoS values obtained for 0.1g, 0.3g and 0.5g for andesitic basaltic tuff, these values are obtained at 16.14, 9.99 and 7.10, while the same values for limestone are 16.14, 35% and 34% with increases of around 33%, 35% and 34%. It is seen that 9.99 and 7.10 were obtained.

Considering that unstable situation for the stability status of the slopes will occur below 1 and it is understood that under the analyzed assumptions, the slope system is stable under both static and pseudo-static loading if it consists of limestone or andesitic basaltic tuff system.

4. Conclusion

Within the scope of this study, a slope section was obtained using photogrammetrically produced point cloud data in the Zigana region of the Gümüşhane-Trabzon highway (5 km Gümüşhane side of the old Zigana Tunnel). Parametric analyzes were carried out for the created slope system to be limestone or andesitic basaltic tuff, which is known to be frequently found in the region. Finite element approach was considered for parametric analyses. Loadings were carried out under static and Pseudo-static loadings. In pseudo-static analyses, the load condition was increased from 0.1g to 0.5g. The data obtained from the analyzes are presented in terms of total displacements obtained from three selected nodes. Additionally, factor of safety values was calculated for static and pseudo-static loading cases. The inferences obtained in this context are listed below.

For cases where the slope system consists of limestone or andesitic basaltic tuff, the displacements obtained from pseudo-static loading can increase significantly within the three nodal points depending on the increase in the loading magnitude.

Displacements can increase significantly due to the decrease in mechanical parameters and unit volume weight of andesitic basaltic tuff compared to limestone for all pseudo-static loading conditions.

When the factor of safety values calculated under the assumptions made are examined, it is understood that the slope system is stable (durable) under both static and pseudo-static loading in cases of limestone or andesitic and basaltic tuff. The change in factor of safety decreases significantly in both cases due to the gradual increase in loadings. It is also noteworthy that factor of safety of the slope created from andesitic basaltic tuff remains relatively lower for all loading conditions compared to limestone.

Author contributions

ŞA was involved in writing, investigation and analysis, KFÖ was involved in conceptualization, validation and writing, MAG was involved in ideating, language checking and editing

Conflicts of interest

The authors declare no conflicts of interest.

Statement of Research and Publication Ethics

Research and publication ethics were complied with in the study.

Acknowledgments

Abstract of this study TUFUAB XII. Presented at the Technical Symposium.

References

Alkan, F. & Dağ, S. (2018). Gümüşhane yöresinde yüzeylenen magmatik kökenli bazı kayaların jeomekanik özellikleri arasındaki ilişkilerin araştırılması. *Uludağ Üniversitesi Mühendislik Fakültesi Dergisi*, *23*(2), 203-216.

Bakır, B. S. & Akış, E. (2005). Analysis of a highway embankment failure associated with the 1999 Düzce, Turkey earthquake. *Soil Dynamics and Earthquake Engineering*, 25(3), 251-260.

Bentley, PLAXIS 2D-Tutorial Manual, 2020

Briaud, J. L. (2013). Geotechnical engineering: unsaturated and saturated soils. John Wiley & Sons.

Çetin, K. Ö., Gökçeoğlu, C., Moss, R. E. S., Ilgaç, M.,Can, G., Çakır, E., Aydın, B. U., Şahin, A., Türkezer, M., Söylemez, B., Ocak, S. & Güzel, H. (2023). Geotechnical Findings and the Performance of Geo-Structures. Kemal Önder Çetin, Makbule Ilgaç, Gizem Can and Elife Çakır (Der.), Preliminary Reconnaissance Report on February 6, 2023, Pazarcık Mw=7.7 and Elbistan Mw=7.6, Kahramanmaraş-Türkiye Earthquakes içinde, Middle East Technical University.

Dawson, E. M., Roth, W. H. & Drescher, A. (1999). Slope stability analysis by strength reduction. Geotechnique, 49(6), 835-840.

Erdik, M. (2001). Report on 1999 Kocaeli and Düzce (Turkey) earthquakes. *In Structural control for civil and infrastructure engineering*, 149-186.

Günen, M. A. & Beşdok, E. (2021). Comparison of point cloud filtering methods with data acquired by photogrammetric method and RGB-D sensors. International Journal of Engineering and Geosciences, 6(3), 125-135.

Kobayashi, Y. (1981). Causes of fatalities in recent earthquakes in Japan. *Natural disaster science*, 3(2), 15-22.

Korkmaz, T. (1988). Maçka-Gürgenağaç (Trabzon) yeni yol şevlerinin duraylılık açısından incelenmesi (Yüksek lisans tezi, Fen Bilimleri Enstitüsü).

Kramer, S. L. (1996). Geotechnical earthquake engineering. Pearson Education India.

Matsui, T. & San, K. C. (1992). Finite element slope stability analysis by shear strength reduction technique. *Soils and foundations*, 32(1), 59-70.

Rusu, R. B., Blodow, N., Marton, Z., Soos, A. & Beetz, M., (2007). Towards 3D object maps for autonomous household robots. IEEE/RSJ international conference on intelligent robots and systems.

Tan, Y., Wang, S., Xu, B. & Zhang, J. (2018). An improved progressive morphological filter for UAV-based photogrammetric point clouds in river bank monitoring. *ISPRS Journal of Photogrammetry and Remote Sensing*, 146, 421-429.

Terzaghi, K. (1950). Mechanism of landslides, Enginnering Geology (Berkeley) Volume.

Youd, T. L. (1978). Major Cause of a Earthquake Damage Is Ground Failure. *Civil Engineering*, 48(4).

Wang, Q., Wu, L., Xu, Z., Tang, H., Wang, R. & Li, F. (2014). A progressive morphological filter for point cloud extracted from UAV images. IEEE Geoscience and Remote Sensing Symposium (s. 2023-2026).

Wilson, R. and Keefer, D. K. (1985). Predicting areal limit of earthquake-induced landsliding, evaluating eathquake hazards in the Los Angeles region-an earth-science perspective. *US Geological Survery Professional Paper,* 1360, 317-345.